



**Radiation Dose Rate Resistivity Degradation in
Ceramic Insulators and Assessment of the
Consequences in Fusion Reactor Applications**

L.J. Perkins

April 1982

UWFDM-469

***FUSION TECHNOLOGY INSTITUTE
UNIVERSITY OF WISCONSIN
MADISON WISCONSIN***

DISCLAIMER

This report was prepared as an account of work sponsored by an agency of the United States Government. Neither the United States Government, nor any agency thereof, nor any of their employees, makes any warranty, express or implied, or assumes any legal liability or responsibility for the accuracy, completeness, or usefulness of any information, apparatus, product, or process disclosed, or represents that its use would not infringe privately owned rights. Reference herein to any specific commercial product, process, or service by trade name, trademark, manufacturer, or otherwise, does not necessarily constitute or imply its endorsement, recommendation, or favoring by the United States Government or any agency thereof. The views and opinions of authors expressed herein do not necessarily state or reflect those of the United States Government or any agency thereof.

**Radiation Dose Rate Resistivity Degradation in
Ceramic Insulators and Assessment of the
Consequences in Fusion Reactor Applications**

L.J. Perkins

Fusion Technology Institute
University of Wisconsin
1500 Engineering Drive
Madison, WI 53706

<http://fti.neep.wisc.edu>

April 1982

UWFDM-469

RADIATION DOSE-RATE RESISTIVITY
DEGRADATION IN CERAMIC INSULATORS
AND ASSESSMENT OF THE CONSEQUENCES
IN FUSION REACTOR APPLICATIONS

L. John Perkins

Fusion Engineering Program
Nuclear Engineering Department
University of Wisconsin
Madison, WI 53706

April 1982

UWFD-469

SYNOPSIS

Under neutron and/or gamma absorbed dose-rates typical of fusion reactor conditions, common ceramic insulators such as Al_2O_3 , MgO , $MgAl_2O_3$, etc., exhibit a significant instantaneous decrease in their DC resistivity. Ceramic insulators in lightly shielded normal-conducting magnets, direct convertors and first wall applications are shown to be the most affected. Depending on conductor design, magnet location, absorbed dose-rate and applied voltages, it is demonstrated that the resulting leakage currents in the ceramic material are potentially capable of producing significant Joule heating rates which may lead to thermal runaway and subsequent insulator destruction.

In section 2, the theoretical background for this effect is presented and the rather sparse experimental data base reviewed.

In section 3, recommendations are given for computing worst case radiation-induced conductivity increases as a function of absorbed dose rate. The possible ameliorating influences of long term fluence damage are then discussed.

In sections 4 and 5, the practical consequences of ceramic resistivity degradation are quantitatively assessed by consideration of resulting leakage current Joule heating in the extruded conductor of a typical normal-conducting magnet. Relationships are derived to compute dose-rate-dependent leakage currents and Joule heating rates as a function of several magnet parameters. In general, the dose-rate-induced Joule heating rate per unit volume is shown to scale as $\sim V_0^2 D_r / \delta^2$ where D_r is the absorbed dose-rate and V_0 is the voltage applied across a characteristic insulator dimension of δ . Finally, the relative contributions of dose-rate-induced Joule heating and direct nuclear heating are assessed in a parametric study which indicates that the magnitude of leakage currents capable of leading to thermal runaway effects

are critically dependent on the design of the magnet or insulator assembly.

ACKNOWLEDGEMENT

It is my pleasure to acknowledge the valuable assistance of Dr. Frank W. Clinard, Jr., of Los Alamos National Laboratory who, through numerous telephone conversations and supplied literature, provided many experimental and theoretical details of dose-rate-dependent conductivity effects in ceramic materials.

CONTENTS

	<u>Page</u>
1. INTRODUCTION	1
2. A REVIEW OF THE EXPERIMENTAL AND THEORETICAL BACKGROUND	4
3. COMPUTATION OF DOSE-RATE DEPENDENT CONDUCTIVITIES	7
3.1 Computational Method	7
3.2 The Influence of Long Term Fluence Effects	10
4. PRACTICAL CONSEQUENCES OF DOSE-RATE CONDUCTIVITY INCREASES	12
4.1 Some Examples of Relevant Fusion Systems	12
4.2 Application to Extruded Magnet Windings	13
4.3 Discussion	18
5. A QUANTITATIVE EXAMPLE OF DOSE-RATE-INDUCED JOULE HEATING	24
5.1 A Representative Conductor Design	24
5.2 Relative Contributions of Nuclear Heating and Dose-Rate-Induced Joule Heating	27
6. CONCLUSIONS AND RECOMMENDATIONS	32
6.1 General Conclusions	32
6.2 Edge-Cooled Ribbon Wound Magnets	32
6.3 Magnets Employing Extruded Ceramic Insulation	33
6.4 Direct Converter Insulators	33
6.5 Methods of Reducing Dose-Rate-Induced Conductivity Effects	34
6.6 The Need for Further Experimental Data	35
REFERENCES	36

1. INTRODUCTION

Current conceptual designs of fusion engineering facilities and power reactors based on the tandem mirror principle have specified the requirement for barrier and/or axicell mirror solenoids producing very high magnetic fields. Requirements for on-axis fields in the range ~ 12 to 28 teslas are typical. For example, in the TASKA tandem mirror fusion engineering facility,⁽¹⁾ barrier fields of 20 T were specified. Similarly, in the Mirror Advanced Reactor Study (MARS)⁽²⁾ and the Tandem Mirror Technology Demonstration Facility Study (TDF)⁽³⁾ currently in progress, mirror fields of $\sim 24 - 28$ T and 15 T, respectively, are required. Due to the critical field limit of present day superconductors, production of these large magnetic fields necessitate the use of hybrid solenoids. In such hybrid designs, an outer superconducting solenoid produces up to ~ 14 T of the required axial field, while a concentric normal-conducting copper insert coil supplies the balance. Although it is economically advantageous to minimize the bore radii of both solenoids for a given axial field, the minimum inner radius for the superconducting coil is determined by the neutron and gamma shielding necessary for reducing nuclear heating, stabilizer resistivity-degradation and organic insulator strength losses to specified design limits. However, current designs for the inner normal-conducting solenoids contemplate their operation with little or no shielding between the first wall and the inner windings of the coil. Requirements arise, therefore, for the identification of potential radiation-induced failure mechanisms and estimations of resulting coil lifetimes.

One feature of high field normal-conducting magnets which has been identified as a critical component in determining coil behavior and lifetime under irradiation is the inorganic ceramic insulation. In the TASKA study⁽¹⁾,

for example, an extruded conductor design employing compacted MgO powder insulation was selected. By contrast, the normal-conducting insert coils for MARS⁽²⁾ and TDF⁽³⁾ will probably utilize solid polycrystalline spinel (MgAl_2O_4).⁽⁴⁾ Other ceramic materials which have been considered for normal-conducting magnet insulation include alumina (Al_2O_3) and silicon nitride (Si_3N_4) (see, for example, Clinard's contribution on ceramics for fusion technology in Ref. 5).

Two major radiation effects have been identified which are potentially capable of limiting the operation and expected lifetimes of these ceramic insulators. First, long term neutron fluence damage induces swelling and, in some cases, microcracking in the ceramic matrix. A review of these effects is given by Clinard,⁽²⁴⁾ while recommendations for neutron fluence limits for the common ceramic materials under fusion reactor conditions can be found in an associated publication.⁽⁶⁾ The second radiation effect is that the DC conductivity of the ceramic insulation can be increased significantly by the concurrent absorption of ionizing radiation. Depending on the conductor design, magnet location and incident radiation levels, the resulting leakage currents in the ceramic material can produce deleteriously large Joule heating rates leading to thermal runaway and subsequent insulator destruction. Note that, unlike long term neutron fluence damage, this latter effect is dependent on the instantaneous neutron and/or gamma dose-rate absorption in the ceramic. It is a potential problem, therefore, as soon as the fusion plasma is brought up to operating power.

In this report, the rather sparse data base for radiation-induced conductivity effects in ceramic materials is reviewed and recommendations are given for computing worst-case radiation-induced conductivity increases as a function of absorbed dose-rate. The consequences of resistivity degradation

and resulting leakage currents are then quantitatively assessed by consideration of resulting Joule heating loads in typical extruded conductor designs.

It should be noted that, in addition to tandem mirror hybrid solenoids, there are several other areas of fusion technology in which ceramic dose-rate conductivity effects need to be assessed. Some examples are:

1. The unshielded normal-conducting magnets with ceramic insulation employed in the limited-lifetime disposable toroidal devices such as the RIGGATRON (see, for example, Bussard and Shanny⁽⁷⁾).
2. Bundle divertor coils which are usually designed to be operated with little or no shielding due to iron ripple losses (see, for example, Schultz⁽¹³⁾).
3. The direct convertors at the end of tandem mirror fusion devices. These convert plasma charged particle energy to DC electricity and employ ceramic insulators with stand-off voltages in the region of tens to hundreds of kV (see, for example, Ref. 22 and 23).
4. Ceramic current breaks in tokamak first walls.
5. Ceramic insulators on the first wall of theta pinch reactors (see, for example, Ref. 19 and 21).

Typical absorbed dose-rates for the ceramics insulators in some of the above will be considered in section 4.

2. A REVIEW OF THE EXPERIMENTAL AND THEORETICAL BACKGROUND

The primary mechanism for the conductivity increase in a ceramic insulator, for a given instantaneous absorbed dose-rate, is that the deposition of neutron and/or gamma ionization energy in the bulk of the ceramic can excite valence electrons across the band gap into the conduction band. At typical operating temperatures for normal-conducting high field magnets (i.e., ~ 50-150°C), thermal excitation of charge carriers will be negligible compared with those produced by any moderate radiation field.

The generation rate of electron hole pairs would be expected to be proportional to the dose-rate, although a fraction of these carrier pairs will undergo germinate recombination. The remainder, while free, increase the conductivity by an amount $\Delta\sigma$ as

$$\Delta\sigma = e(n_n\mu_n + n_p\mu_p) \quad (1)$$

where n_n, n_p = electron, hole number densities
 μ_n, μ_p = electron, hole mobilities
 e = electronic charge.

Loss of these charge carriers will mainly occur from electron-hole recombination and trapping at defect sites.

Van Lint et al.⁽¹⁹⁾ have examined these recombination effects and concluded that the conductivity increase $\Delta\sigma$ is proportional to dose-rate with a proportionality constant k in the range 10^{-9} to 10^{-13} $(\Omega m)^{-1}/(\text{Gy/s})$.* Note, however, that k is a function of both the temperature and accumulated fluence

* $1 \text{ Gy/s} = 10^2 \text{ rads/s}$

damage (see later).

Davis⁽⁸⁾ measured the conductivity of a number of solid ceramics in a gamma field of $\sim 1.4 \times 10^3$ rad/s (14 Gy/s) and found conductivity increases of $\sim 10^3$. For powdered ceramics, conductivity increases appear to be approximately an order of magnitude worse for the same absorbed-dose. For example, Lynch⁽⁹⁾ reports a factor of 10^3 increase in the DC conductivity of powdered MgO at 475 K for a gamma dose rate of only $\sim 10^2$ rads/s (1 Gy/s). Clinard⁽¹⁸⁾ suggests that the degraded electrical performance of powdered ceramics may, in part, be due to ionization of the trapped compressed gas in the sintered powder matrix.

Klaffky et al.⁽¹¹⁾ have measured the radiation-induced conductivity of single crystal Al₂O₃ (alumina) as a function of temperature and dose-rate. Their results are summarized in Fig. 1. It can be seen that Van Lint's prescription of a linear dependence of conductivity-increase with ionizing dose-rate is reasonably well obeyed, especially around T = 200°C.

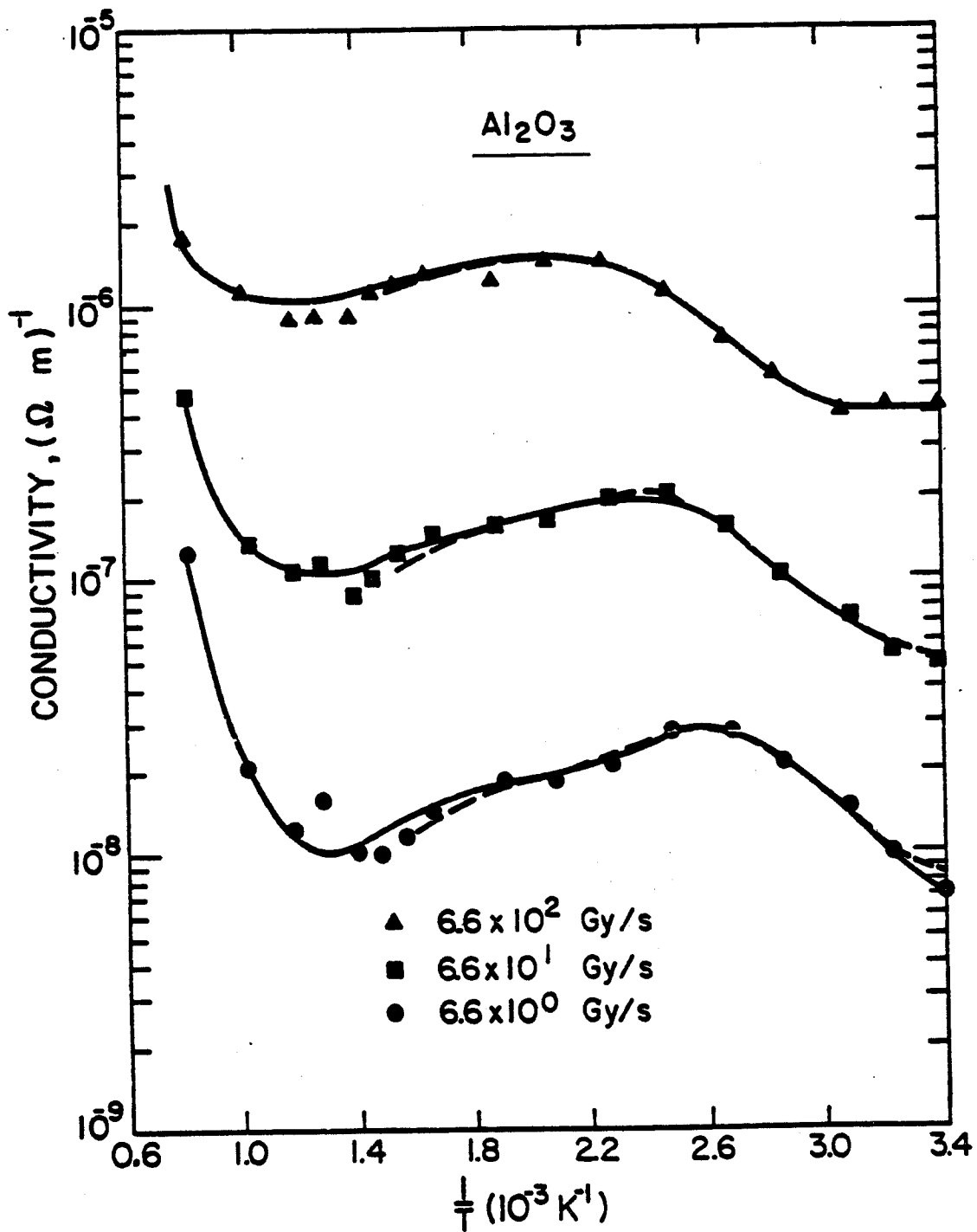


Figure 1 The dependence of radiation-induced conductivity in single-crystal Al₂O₃ on absorbed dose rate and temperature (from Klaffky, et al. (11)).

3. COMPUTATION OF DOSE-RATE DEPENDENT CONDUCTIVITIES

3.1 Computational Method

In view of the fact that very little experimental data is available on radiation-induced conductivity increases in ceramics, especially at high dose rates, it is recommended that, following Van Lint, a conductivity increase proportional to dose-rate be assumed. Proportionality constants will be determined from Klaffky's results for solid Al_2O_3 and, due to the lack of any further experimental evidence, will be assumed to apply to those common ceramics with initial high resistivities (e.g., MgO , Al_2O_3 , $MgAl_2O_4$, Si_3N_4 but not SiC). In addition, a worst case analysis should take into account the additional dose-rate resistivity degradations encountered in powdered ceramics (see above). Accordingly, the following algorithm is suggested:

$$\Delta\sigma(D_r) = f k(T, \phi t) D_r \quad (2)$$

where $\Delta\sigma$ = conductivity increase in $(\Omega m)^{-1}$

$k(T, \phi t)$ = proportionality constant, a function of both temperature T
and neutron fluence $\phi(E_n) \cdot t$

D_r = absorbed dose-rate in Gy/s (1 Gy/s = 10^2 rads/s)

f = powdered ceramic enhancement factor = 10 for sintered powdered ceramics

= 1 for solid ceramics.

The following values of k , averaged from Klaffky's results above, are suggested:

$k(T=20^{\circ}\text{C},0)$	=	8.10×10^{-10}	$(\Omega\text{m})^{-1}/(\text{Gy/s})$
$k(T=60^{\circ}\text{C},0)$	=	1.42×10^{-9}	$(\Omega\text{m})^{-1}/(\text{Gy/s})$
$k(T=100^{\circ}\text{C},0)$	=	2.42×10^{-9}	$(\Omega\text{m})^{-1}/(\text{Gy/s})$
$k(T=200^{\circ}\text{C},0)$	=	2.58×10^{-9}	$(\Omega\text{m})^{-1}/(\text{Gy/s})$

Although more precise values can be obtained by a parametric least-squares fit to the data in Fig. 1, this is not really warranted in view of the present uncertainties in the data base. This is particularly true when applying equation 2 to other ceramics in different configurations and under different conditions (see section 6.6 for further discussion).

The value of the steady state conductivity σ under irradiation is, therefore,

$$\sigma(D_r) = \sigma_0 + \Delta\sigma(D_r) \quad (3)$$

where σ_0 = initial unirradiated conductivity. However, for common ceramics (MgO , Al_2O_3 , MgAl_2O_4 , etc.), values of σ_0 in the range 10^{-10} - $10^{-13} (\Omega\text{m})^{-1}$ are typical.⁽¹²⁾ Therefore, in radiation fields resulting in absorbed dose-rates greater than ~ 0.1 Gy/s (10 rads/s), the steady state conductivity under irradiation (i.e., the reciprocal of the dose-rate degraded resistivity) will be given by equation 2.

Fig. 2 illustrates the dose-rate degraded resistivity expressed by equations 2 and 3, where the ceramic resistivity $\rho_I(D_r)$ is plotted as a function of the absorbed dose rate D_r for constant irradiation temperatures of 20°C , 60°C and 100°C . The shaded region indicates the regime for non-irradiated ceramics where typical resistivities are in the region of $\sim 10^{10}$ - $10^{13} \Omega\text{m}$ (see above).

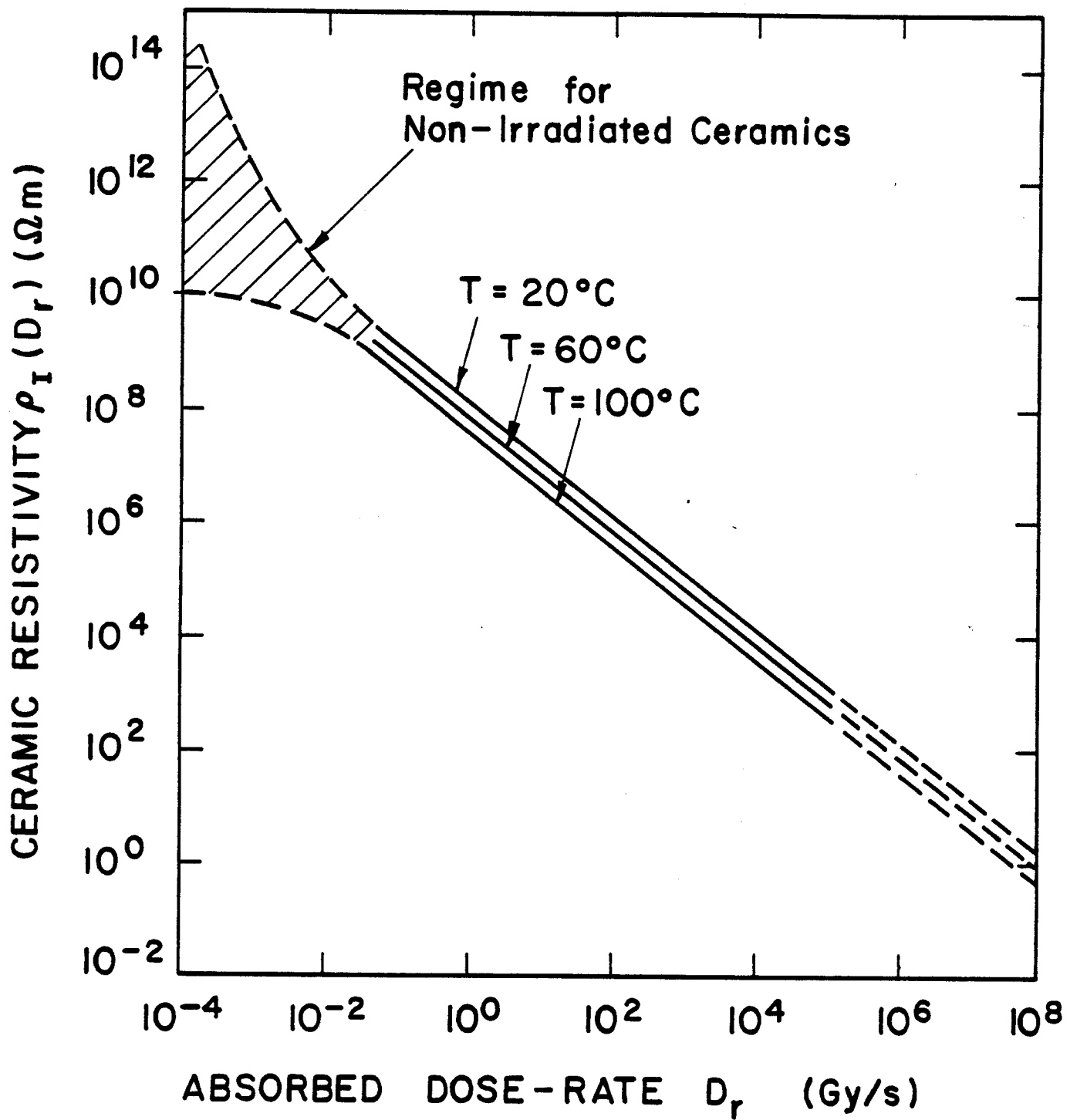


Figure 2 Radiation-degraded resistivity of a representative ceramic insulator as a function of absorbed dose-rate.

3.2 The Influence of Long Term Fluence Effects

It was noted above that k is a function of both temperature T and neutron fluence damage $\phi(E_n) \cdot t$. Long term fluence will promote structural changes within the material which are capable of altering the electronic properties of the insulator. Introduction of trapping, recombination or scattering centers will increase the resistivity at any instantaneous absorbed dose-rate, while defect states produced within the band gap will have the opposite effect.

For the common ceramic materials, the effect of long term fluence damage is expected to be generally beneficial in respect of reducing dose-rate effects.⁽¹⁰⁾ For example, samples of Al_2O_3 , previously irradiated in neutron fluences of $\sim 10^{22} \text{ n cm}^{-2}$, exhibited instantaneous dose-rate conductivities of approximately two orders of magnitude less than previously unirradiated samples.⁽¹⁵⁾

Although long term fluence appears to reduce instantaneous dose-rate conductivity effects, many ceramic materials exhibit drastic decreases in thermal conductivity under long term irradiation. This is due to the fact that radiation-induced defects are capable of scattering phonons by which heat is conducted. In the case of Al_2O_3 , for example, room temperature thermal conductivity is reduced $\sim 70\%$ by an accumulated fluence of $\sim 10^{22} \text{ n cm}^{-2}$ ($E > 0.1 \text{ MeV}$) performed at 925 K.⁽¹⁶⁾ Lower irradiation temperatures result in a greater degradation of this property. Thermal conductivities of MgO and Si_3N_4 are similarly significantly reduced^(16,17) in fluences of $\sim 10^{22} \text{ n cm}^{-2}$ ($E > 0.1 \text{ MeV}$). One exception to this trend appears to be MgAl_2O_4 (spinel). This has inherently good neutron damage resistance and, in single-crystal form, exhibits essentially no change in thermal conductivity⁽¹⁶⁾ after irradiation to $\sim 10^{22} \text{ n cm}^{-2}$ at 925 K and 1100 K. In polycrystalline form, spinel exhibits $\sim 30\%$ reduction in thermal conductivity under the same

irradiation conditions.⁽¹⁶⁾ Decrease in thermal conductivity is an important consideration in assessing the consequences of dose-rate-induced electrical conductivity effects, since it will exacerbate thermal runaway effects in the insulator (see later).

4. PRACTICAL CONSEQUENCES OF DOSE-RATE CONDUCTIVITY INCREASES

4.1 Some Examples of Relevant Fusion Systems

It is now instructive to assess ceramic dose-rate conductivity increases in three typical fusion irradiation situations as follows:

1. The unshielded normal-conducting insert coil for the MARS hybrid mirror solenoid.⁽²⁾

A 1-D neutronics analysis for a preliminary design of this coil,⁽²⁰⁾ for a fusion wall loading of 4 MW m^{-2} , yielded a peak absorbed dose-rate in the spinel (MgAl_2O_4) insulator of $\sim 8.15 \times 10^3 \text{ Gy/s}$ ($8.15 \times 10^5 \text{ rads/s}$). Applying equation 2 at a temperature of 100°C (a typical coil operating temperature) gives $\Delta\sigma \approx \sigma = 1.98 \times 10^{-4} (\Omega\text{m})^{-1}$. This is equivalent to a worst case radiation-induced resistivity of $5.05 \times 10^3 \Omega\text{m}$.

2. A conceptual design for the unshielded ETF bundle divertor coil.⁽¹³⁾ According to Schultz,⁽¹³⁾ the powdered MgO insulator sustains an absorbed dose-rate of $\sim 5 \times 10^4 \text{ Gy/s}$ per MW m^{-2} of wall loading. From equation 2 for $T = 100^\circ\text{C}$, a worst case radiation-induced resistivity of $8.26 \times 10^2 \Omega\text{m}$ per MW m^{-2} of wall loading will result.
3. The first wall ceramic insulator in the reference design of the Reverse Theta Pinch Reactor (RTPR).⁽²¹⁾

During the 0.1 s thermonuclear burn, this insulator is subjected to an instantaneous dose-rate of $\sim 7 \times 10^6 \text{ Gy/s}$. At this time, the ceramic is not required to retain its insulating properties. However 10 s later it must withstand the electrical stress of the next implosion-heating pulse. At that time, the residual ionization dose-rate is down to $\sim 2 \times 10^2 \text{ Gy/s}$. Again from equation 2, this translates to a worst case degraded resistivity of $\sim 2.07 \times 10^5 \Omega\text{m}$.

One might now ask: so what? The worst case radiation-induced resistivities above are still apparently a factor of $\sim 10^{10} - 10^{12}$ greater than the resistivity of typical copper conductors at this temperature (the resistivity of pure Cu at 100°C is $2.24 \times 10^{-8} \Omega\text{m}$, while that of OFHC hardened Cu is $\sim 3.29 \times 10^{-8} \Omega\text{m}$). The consequences are, however, very important with respect to the leakage currents and resulting Joule heating in the ceramic insulation. As will be seen in the next subsection, this is especially true for the more conventional types of high field normal-conducting magnets which are wound with a one-piece extruded conductor.

4.2 Application to Extruded Magnet Windings

Fig. 3 is a schematic view of a square-section extruded magnet winding. The winding is seen to consist of a central copper alloy conductor with integral water cooling channel, surrounded by an insulating layer of MgO compacted powder ceramic. A metallic outer sheath is included for structural integrity. The power supply voltage V_0 is applied across the conductor as shown, while the outer sheath is operated at ground potential.

The series resistance of the copper conductor between its ends is

$$R_C = \rho_C \frac{\ell}{b^2 - A_W} \quad (4)$$

where

ρ_C = conductor resistivity

ℓ = winding length

$b \times b$ = cross sectional dimensions of conductor

A_W = cross sectional area of coolant channel.

The total Joule heating rate in the conductor is thus simply

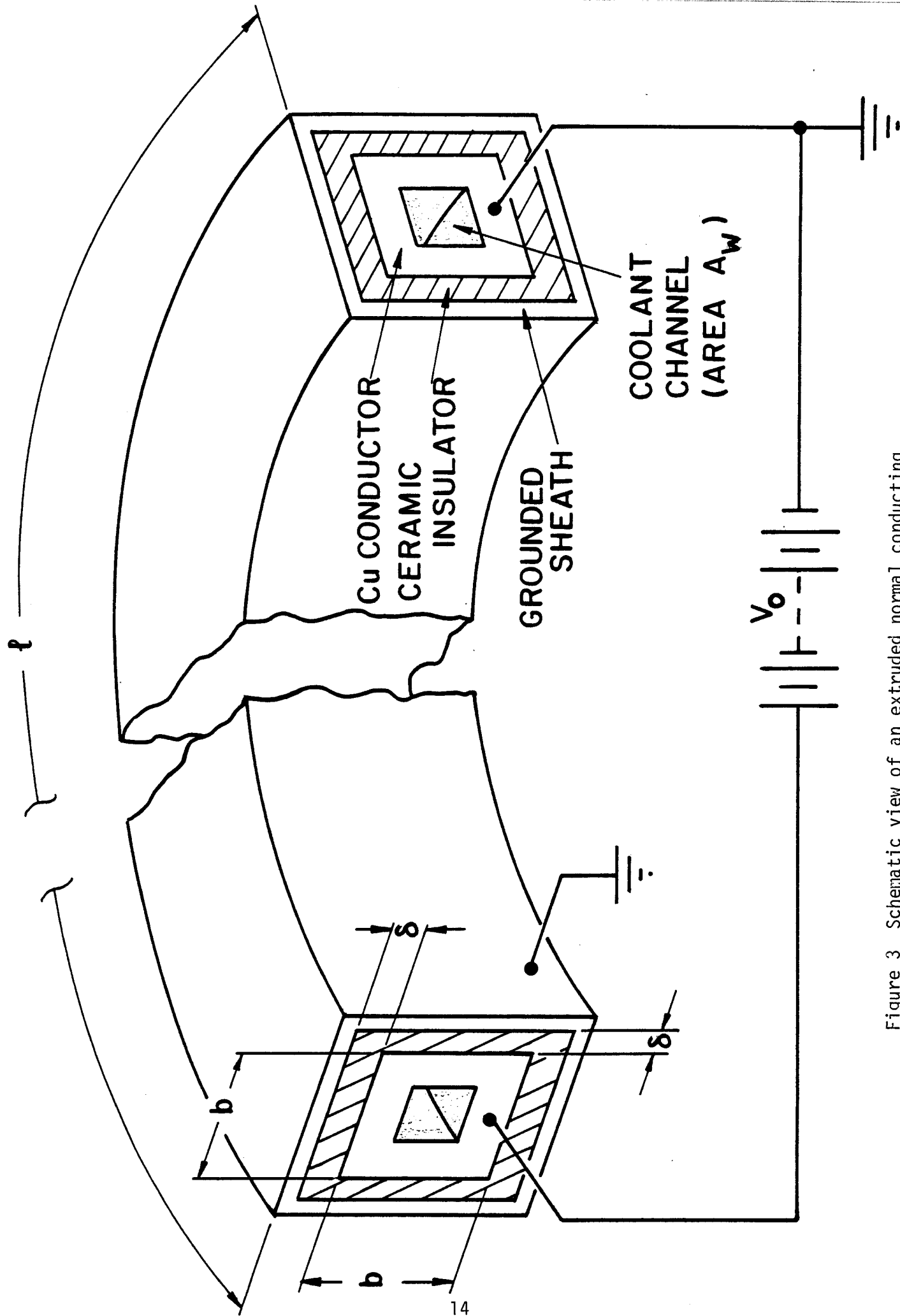


Figure 3 Schematic view of an extruded normal conducting magnet winding. The power supply voltage V_0 is applied across the ends of the conductor. The outer sheath is at ground potential.

$$W_c = V_0^2 / R_c = \frac{V_0^2}{\rho_c \ell} (b^2 - A_w) . \quad (5)$$

In the case of radiation-induced resistivity degradations in the ceramic insulator, it is necessary to consider leakage currents flowing across the insulator from the central conductor to the grounded outer sheath. However, the potential difference across the insulator is V_0 at one end and zero at the other, with a distribution $V(x)$ as a function of x along the length of the conductor given by

$$V(x) = V_0 (1 - x/\ell) . \quad (6)$$

Consider an incremental length dx of winding at a distance x from the supply terminal at V_0 . The insulator conductance of this incremental section is

$$dC_I(D_r) = 4\sigma_I(D_r) \frac{b}{\delta} dx \quad (7)$$

where

δ = insulator thickness

$\sigma_I(D_r)$ = insulator conductivity which is a function of the absorbed dose-rate D_r

and where, to a good approximation, this shunt conductance is taken to be four slabs of insulator of cross-sectional area $b dx$ and thickness δ connected in parallel. The resulting Joule heating rate in this incremental section of ceramic is, therefore,

$$dW_I(D_r, x) = V^2(x) dC_I(D_r) . \quad (8)$$

Substituting for $V(x)$ from equation 6 and for dC_I from 7, and integrating over the length ℓ of the winding gives the total Joule heating rate in the insulator as

$$W_I(D_r) = \int_0^{\ell} dW_I(D_r, x) = \frac{4}{3} \sigma_I(D_r) \frac{V_0^2 b \ell}{\delta} . \quad (9)$$

Making the substitution from conductivity to resistivity as

$$\rho_I(D_r) = 1/\sigma_I(D_r) \quad (10)$$

and dividing by equation 5, yields the ratio of the Joule heating rate in the ceramic to that in the conductor as

$$\frac{W_I}{W_C}(D_r) = \frac{4}{3} \frac{\rho_C}{\rho_I(D_r)} \frac{b \ell^2}{\delta(b^2 - A_w)} \quad (11)$$

where ρ_C = conductor resistivity

$\rho_I(D_r)$ = insulator resistivity (a function of the dose-rate D_r)

ℓ = winding length

$b \times b$ = cross-sectional dimensions of conductor

A_w = cross-sectional area of coolant channel

δ = insulator thickness.

Equation 11 can be expressed explicitly in terms of the dose-rate D_r by substituting for $\rho_I(D_r)$ from equations 2 and 10, thus

$$\frac{W_I}{W_C}(D_r) = \frac{4}{3} \rho_C \frac{b \ell^2}{\delta} \frac{fk(T, \phi t) D_r}{b^2 - A_w} \quad (12)$$

where f , $k(T, \phi t)$ and D_r are defined in equation 2.

Possibly a more interesting parameter for the ceramic is not the total Joule heating rate $W_I(D_r)$ but the Joule heating rate per unit volume, $W_{IV}(D_r, x)$, which is a function of position x along the winding length. Accordingly, dividing equation 8 by the ceramic differential volume $4\delta b dx$ and substituting for dC_I and $V^2(x)$ yields the insulator Joule heating rate per unit volume as

$$W_{IV}(D_r, x) = \frac{V_0^2}{\rho_I(D_r)\delta^2} (1 - x/\ell)^2 . \quad (13)$$

This has a maximum value at the supply voltage end of the winding (i.e., at $x = 0$) of

$$W_{IV}^{\max}(D_r) = \frac{V_0^2}{\rho_I(D_r)\delta^2} . \quad (14)$$

Explicitly in terms of the dose-rate, D_r , this becomes

$$W_{IV}^{\max}(D_r) = \frac{V_0^2}{\delta^2} f k(T, \phi t) D_r . \quad (15)$$

Finally, dividing equation 13 by the Joule heating rate per unit volume in the conductor ($W_{CV} = V_0^2/(\rho_C \ell^2)$) gives the ratio of Joule heating rates per unit volume in the insulator and conductor as

$$\frac{W_{IV}}{W_{CV}}(D_r, x) = \frac{\rho_C}{\rho_I(D_r)} \frac{(\ell-x)^2}{\delta^2} \quad (16)$$

which has a maximum value at $x = 0$ of

$$\frac{W_{I_V \text{ max}}}{W_{C_V}} (D_r) = \frac{\rho_C}{\rho_I(D_r)} \frac{\ell^2}{\delta^2} \cdot \quad (17)$$

Explicitly in terms of dose-rate, this becomes

$$\frac{W_{I_V \text{ max}}}{W_{C_V}} (D_r) = \rho_C \ell^2 f k(T, \phi t) D_r / \delta^2 \quad (18)$$

4.3 Discussion

Consider the implications of equations 11 through 18. From equation 11, it can be seen that, for a given supply voltage V_0 and dose-rate degraded ceramic resistivity $\rho_I (D_r)$, the ratio of the Joule heating rate in the ceramic insulator to that in the conductor increases as the square of the winding length ℓ . The same comment applies to the maximum value of the ratio of the Joule heating rates per unit volume from equation 17. Now one method of reducing Joule heating in the conductor winding is to increase the winding length ℓ for the same supply voltage V_0 .^{*} Since the winding current decreases as $1/\ell$, the power dissipation decreases at the same rate, while the total ampere-turns per unit length are conserved (increasing the winding length for constant V_0 is equivalent to decreasing the current density while increasing the winding cross section). However, while the conductor Joule heating is decreasing for increasing length, that for the insulator is increasing due to the increasing cross sectional area of the shunt resistance (see equation 7). The net result is an increase in W_I/W_C or $W_{I_V}/W_{I_C} (\text{max})$ which scales as ℓ^2 .

^{*}Note that in the conceptual design of the MARS tandem mirror reactor,⁽²⁾ conductor Joule heating rates in the normal-conducting inserts of the hybrid mirror solenoids will be in the range of 50-100 MW! Therefore, during coil design optimization, there is a strong incentive to minimize this conductor power dissipation.

The most important parameter for the ceramic insulator is the maximum Joule heating rate per unit volume, given by equation 14 or 15. In view of the fact that the thermal conductivity of typical MgO ceramic insulation material is only $\sim 1/166$ that of Cu at room temperature,⁽¹⁴⁾ there exists a maximum heating rate in the ceramic, above which thermal runaway effects will result in insulator breakdown. Under thermal runaway, the radiation-induced Joule heating load in the ceramic cannot be accommodated by the magnet coolant flow. The resulting deleterious temperature rise in the insulator leads to thermal excitation of additional charge carriers which contribute to additional Joule heating in the insulator, thus stimulating further charge-carrier release in a positive feedback mode. The onset of thermal runaway effects can be seen in Fig. 1 where there is a large increase in conductivity for temperatures greater than ~ 1000 K.

With regard to thermal runaway, it is important to note that the total heating rate in the ceramic insulator includes contributions from both Joule heating due to dose-rate-induced leakage currents and nuclear heating from the absorbed dose-rate directly. Since the absorbed dose-rate is simply the energy deposited per second per unit mass of material, the nuclear heating rate per unit volume in the insulator is, therefore,

$$W_{IV}^N (D_r) = \epsilon D_r \quad (19)$$

where ϵ is the ceramic density. Accordingly, combining equations 15 and 19, the maximum value of the total heating rate per unit volume of insulator is

$$\begin{aligned}
W_{IV}^{\text{total}}(D_r) &= \text{Maximum dose-rate-induced Joule heating rate per unit volume} & + & \text{Nuclear heating rate per unit volume} \\
&= (W_{IV}^{\text{max}}(D_r)) & & (W_{IV}^N(D_r))
\end{aligned}$$

i.e.,

$$W_{IV}^{\text{total}}(D_r) = D_r \left(\frac{V_0^2}{\delta^2} f k(T, \phi t) + \epsilon \right) . \quad (20)$$

Just which of these two heating rates will dominate depends on the relative values of $V_0^2 f k(T, \phi t) / \delta^2$ and ϵ as follows:

If

$$V_0^2 f k(T, \phi t) / \delta^2 > \epsilon , \quad (21)$$

then dose-rate-induced Joule heating is the dominant effect. If

$$V_0^2 f k(T, \phi t) / \delta < \epsilon , \quad (22)$$

then nuclear heating is the dominant effect. This will be considered further in the next section.

One final parameter of interest is the magnitude of the leakage currents flowing in the insulator. Accordingly, employing equation 7, the incremental current $dI_I(x)$ flowing across the differential portion of insulator of length dx at a position x along the conductor length is

$$dI_I(D_r, x) = V(x) dC_I(D_r) = 4 V(x) \sigma_I(D_r) \frac{b}{\delta} dx . \quad (23)$$

Integrating along the length ℓ of the winding gives the total dose-rate-induced leakage current flowing across the insulator as

$$I_I (D_r) = \frac{2bV_0}{\delta} \frac{\ell}{\rho_I(D_r)} \cdot \quad (24)$$

Explicitly in terms of dose-rate, D_r , this becomes

$$I_I (D_r) = 2 f k(T, \phi t) D_r \frac{b}{\delta} V_0 \ell \cdot \quad (25)$$

The conventional current flowing in the conductor winding is

$$I_C = V_0/R_C$$

where V_0 is the supply voltage and R_C is the total conductor winding resistance. Accordingly, dividing equation 25 by I_C and substituting for R_C from equation 4 yields the ratio of the total leakage current in the insulator to the conventional current in the conductor winding as

$$\frac{I_I}{I_C} (D_r) = 2 \rho_C f k(T, \phi t) D_r \frac{b\ell^2}{\delta(b^2 - A_w)} \cdot \quad (26)$$

Note that the leakage current in the insulator becomes comparable to the conductor supply current when the winding length approaches:

$$\ell (D_r) \sim \left(\frac{\delta(b^2 - A_w)}{2 \rho_C f k(T, \phi t) D_r b} \right)^{1/2} \quad (27)$$

For convenience, a definition of the symbols employed in equations 2 through 27 follows below:

D_r	=	absorbed dose-rate (Gy/s)
f	=	powdered ceramic enhancement factor
$k(T, \phi t)$	=	conductivity - dose-rate proportionality constant (see equation 2)
$\sigma(D_r)$	=	dose-rate-dependent conductivity $((\Omega m)^{-1})$
$\rho(D_r)$	=	dose-rate-dependent resistivity (Ωm)
l	=	length of magnet winding
x	=	length variable in winding direction measured from $x = 0$ at the supply voltage V_0
bxb	=	cross sectional area of conductor
A_w	=	cross sectional area of coolant channel
δ	=	insulator thickness (see Fig. 3)
V_0	=	power supply voltage
R_c	=	resistance of conductor winding
C	=	conductance (Ω^{-1})
W_I	=	Joule heating rate in insulator due to leakage currents
W_C	=	Joule heating rate in conductor
W_{I_V}	=	Joule heating rate per unit volume in insulator due to leakage currents
W_{I_C}	=	Joule heating rate per unit volume in conductor
ϵ	=	density of ceramic insulator
$W_{I_V}^N$	=	nuclear heating rate per unit volume in insulator

- $W_{I_V}^{\text{total}}$ = maximum value of the total heating rate per unit volume in insulator (due to both nuclear heating and leakage current Joule heating)
- $I_I(D_r)$ = dose-rate dependent leakage current in insulator
- I_C = magnet supply current in conductor winding

5. A QUANTITATIVE EXAMPLE OF DOSE-RATE INDUCED JOULE HEATING

5.1 A Representative Conductor Design

For a quantitative assessment of the implications of equations 11 through 18, consider Fig. 4. This illustrates a cross section of the conceptual magnet winding for the ETF bundle divertor taken from Schultz,⁽¹³⁾ and represents a typical extruded conductor design.

Substituting the dimensions from Fig. 4 into Equations 17 and 18 gives the maximum value for the ratio of Joule heating rates per unit volume of insulator to conductor as

$$\frac{W_{IV} \max}{W_{CV}} (D_r) = 1.14 \times 10^{-2} \frac{\ell^2}{\rho_I(D_r)} = 2.75 \times 10^{-10} D_r \ell^2 \quad (28)$$

where ℓ is in meters, D_r is in Gy/s, and where ρ_c and $K(T,0)$ have been evaluated at 100°C which is assumed to be a suitable upper bound for the magnet operating temperature.

Fig. 5 graphs equation 28, where W_{IV}/W_{CV} is plotted as a function of the conductor length ℓ for constant values of the absorbed dose-rate D_r . The shaded area indicates the regime for non-irradiated ceramics (i.e., $D_r = 0$), where values of unirradiated resistivities are typically in the range 10^{10} to $10^{13} \Omega\text{m}$.⁽¹²⁾ The consequences of dose-rate resistivity degradations are now clearly seen. For example, an absorbed dose of $\sim 10^5$ Gy/s yields an insulator/conductor resistivity ratio of 1.25×10^{10} , apparently a very large difference. However, a winding length of only ~ 180 m of the conductor shown in Figure 4 would be required for equal values of the maximum Joule heating rates per unit volume in the insulator and conductor. Computing the length of winding required for equal currents in the insulator (leakage) and conductor, via equation 27, yields $\ell \sim 440$ m. It would appear, therefore, that the

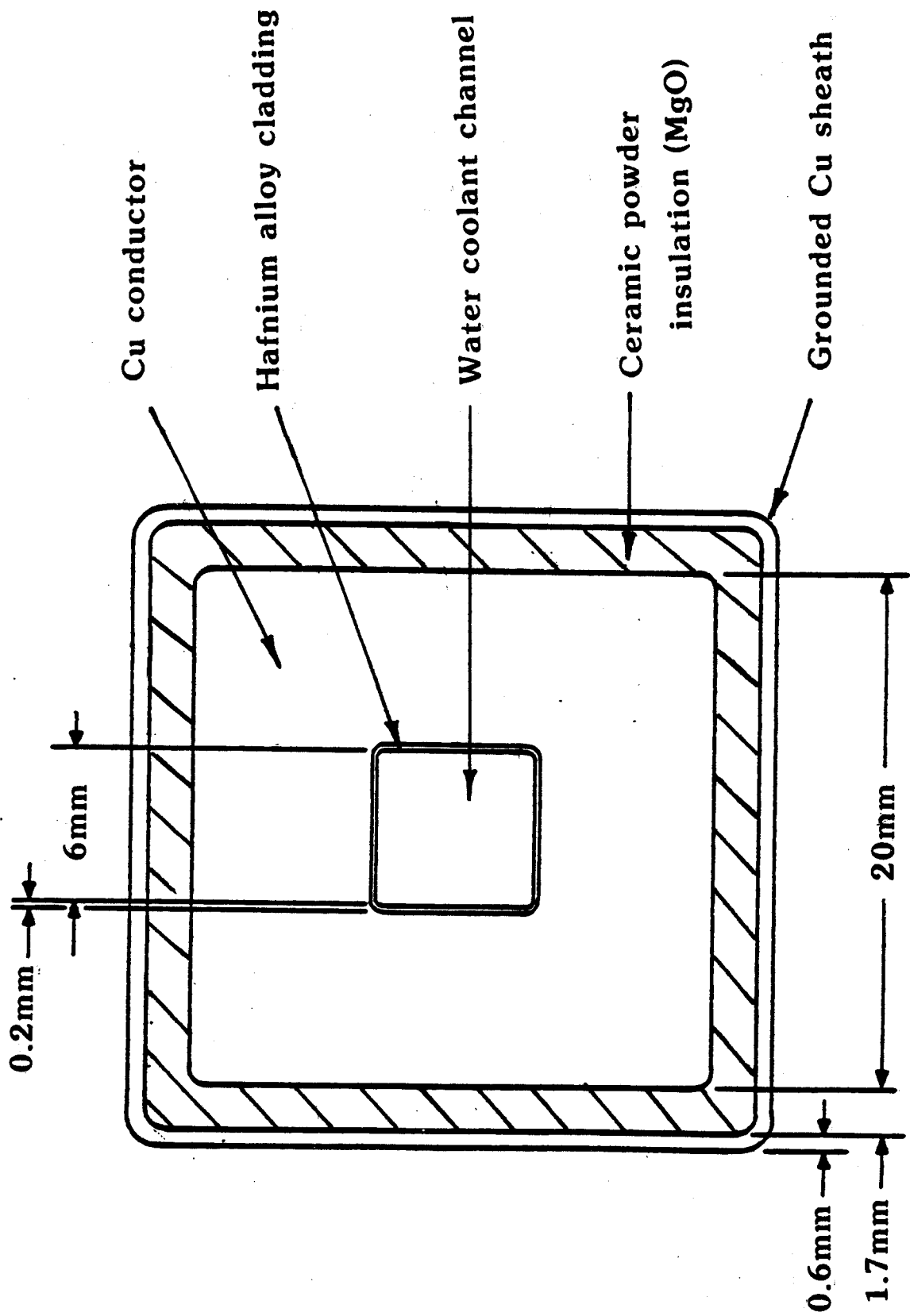


Figure 4 Cross section of a typical extruded magnet winding. This is a conceptual conductor design for an ETF bundle divertor coil from Schultz.

MAXIMUM JOULE HEATING RATE PER UNIT VOLUME OF INSULATOR
 JOULE HEATING RATE PER UNIT VOLUME OF CONDUCTOR

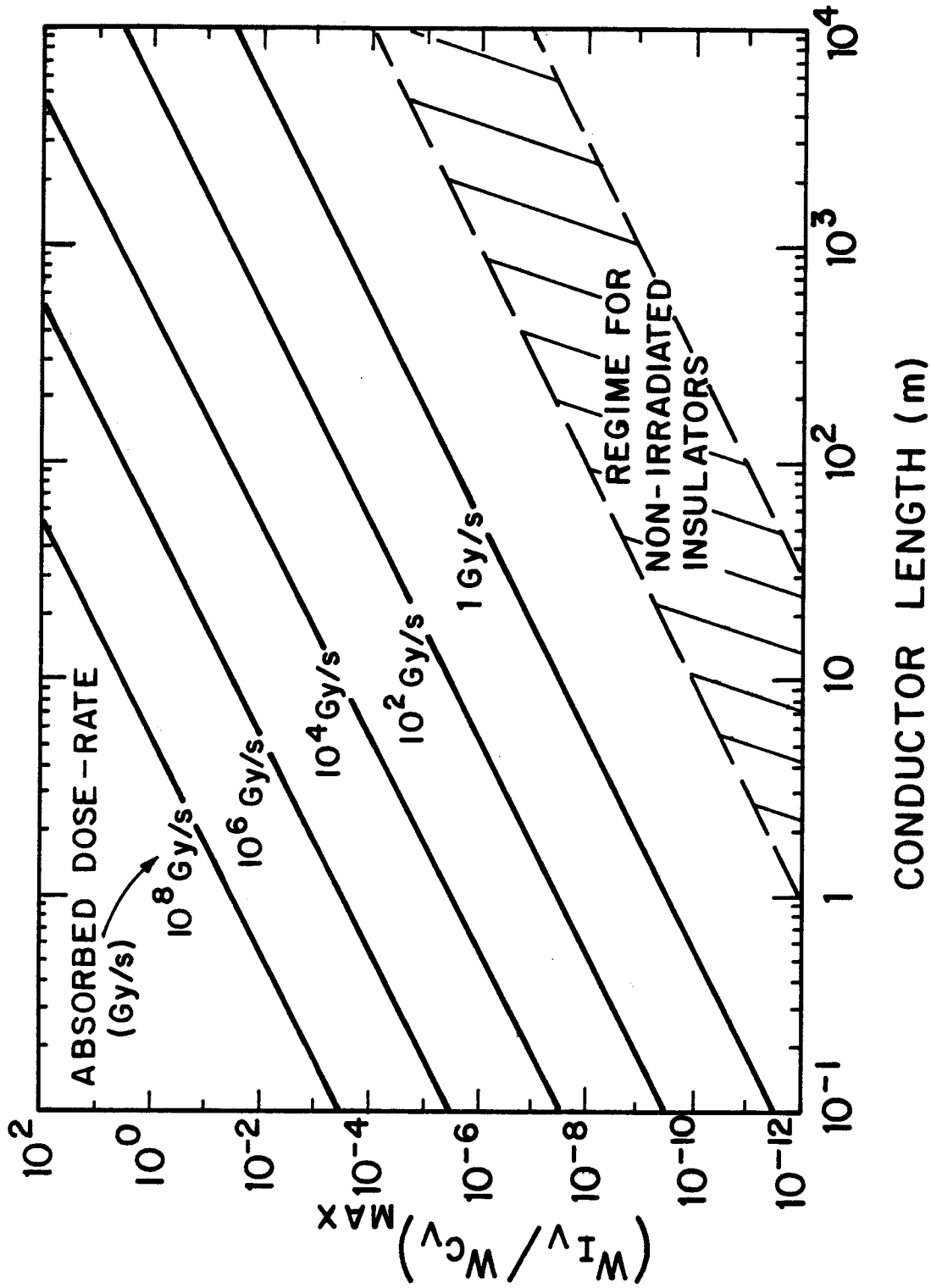


Figure 5 Ratio of the Joule heating rates per unit volume in the ceramic insulator and conductor as a function of the winding length with the absorbed dose-rate in the insulator as a parameter.

leakage current drain on magnet power supplies is unlikely to be a problem except for very long winding lengths or very high absorbed dose-rates. This computation of the leakage current assumes that all the insulation is subject to the same absorbed dose-rate. In reality, inner layers of the coil comprise an effective radiation shield for the outer layers, thereby reducing the absorbed dose-rate in the latter. This factor will be discussed further in section 6.5.

5.2 The Relative Contributions of Nuclear Heating and Dose-Rate-Induced Joule Heating

As discussed in section 5, the most important parameter to compute for a particular magnet design is the maximum value of the heating rate per unit volume in the ceramic insulator. As shown above, this heating rate has contributions from both dose-rate-induced Joule heating and direct nuclear heating. Substituting the dimensions from Fig. 4 into equations 14 and 15 yields the Joule heating contribution as

$$w_{IV}^{\max}(D_r) = 3.46 \times 10^{-1} \frac{V_0^2}{\rho_I(D_r)} = 8.37 \times 10^{-9} V_0^2 D_r \quad (29)$$

where w_{IV}^{\max} is in units of $W \text{ cm}^{-3}$, D_r is in Gy/s, V_0 is in volts and where temperature dependent parameters have been evaluated at 100°C (see above).

Equation 29 above is for radiation-induced Joule heating only. To compute the total heating (i.e., radiation-induced Joule heating plus nuclear heating) equation 20 must be employed. Accordingly, substituting the parameters from Fig. 4 into equation 20 together with a typical value for the

density of the powdered MgO insulator of 3.22 g/cm^3 * yields the maximum value of the total heating rate per unit volume of insulator as

$$w_{IV}^{\text{total}}(D_r) = D_r (8.37 \times 10^{-9} V_0^2 + 3.22 \times 10^{-3}) \quad (30)$$

where, as above, w_{IV}^{total} is in units of W cm^{-3} .

Figures 6 and 7 graph equations 29 and 30, respectively. In Fig. 6, the maximum heating rate per unit volume in the insulator due to radiation-induced Joule heating only is plotted as a function of the terminal supply voltage V_0 for constant values of the absorbed dose-rate D_r . The shaded area indicates the regime for non-irradiated ceramics. In Fig. 7 the maximum value of the total heating rate per unit volume in the insulator, due to both radiation-induced Joule heating and nuclear heating, is plotted as a function of the terminal supply voltage V_0 for constant values of the absorbed dose-rate D_r .

It can be seen from Fig. 7 that, at low terminal voltages, the dominant contribution to the total heating rate comes from nuclear heating alone as evidenced by the flat portion of the curves. At higher terminal voltages, the plots begin to turn upwards showing the increasing contribution of radiation-induced Joule heating which scales as V_0^2 .

The relative contribution of the two heating methods is expressed by the relationships in equations 21 and 22. Both donate an equal contribution when

*This value is obtained from the density of solid MgO (3.58 g/cm^3) with the assumption of a typical packing fraction of 90%.

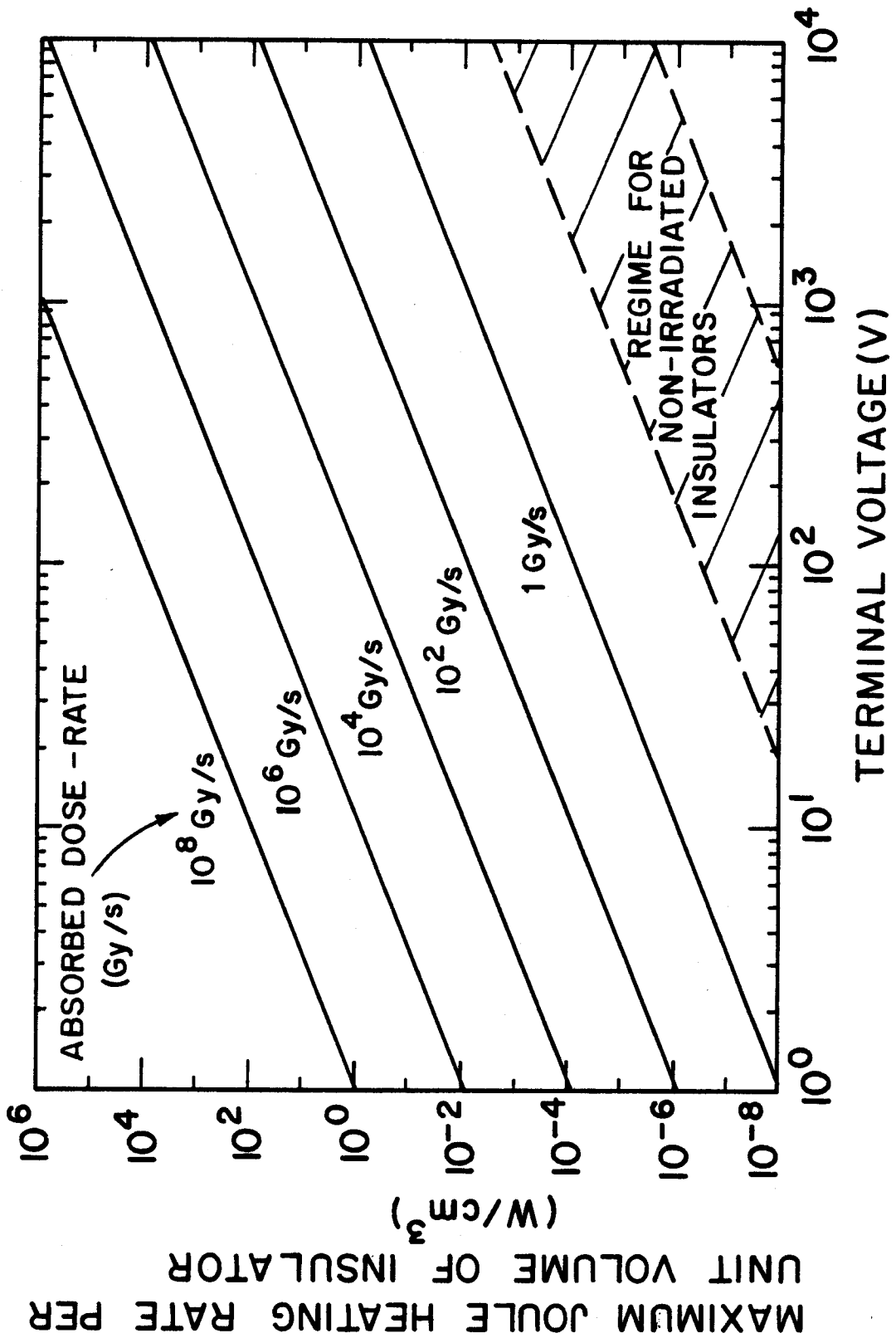


Figure 6 Maximum value of the Joule heating rate per unit volume in the ceramic insulator due to radiation-induced leakage currents as a function of the terminal supply voltage. The absorbed dose-rate in the insulator is shown as a constant parameter.

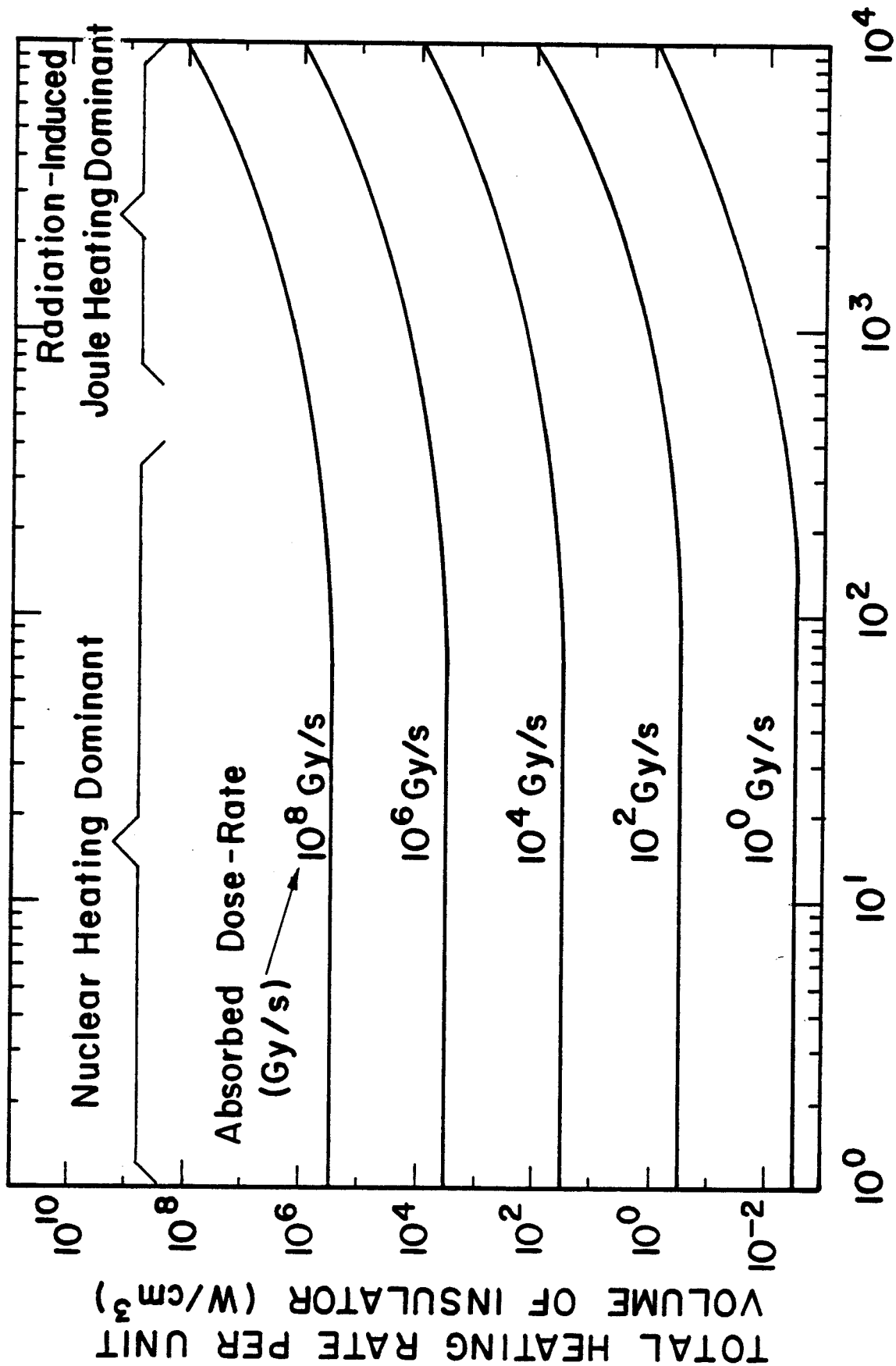


Figure 7 The maximum value of the total heating rate per unit volume in the ceramic insulator as a function of the terminal supply voltage with the absorbed dose-rate in the insulator as a parameter. This total heating rate is composed of direct nuclear heating and dose-rate-induced Joule heating due to leakage currents. The relative contributions of these two components are indicated.

$$V_0 = \left(\frac{\epsilon \delta^2}{f K(T, \phi t)} \right)^{1/2} . \quad (31)$$

Solving this for the conductor design in Fig. 4 for $T = 100^\circ\text{C}$ gives

$$V_0 = 620 \text{ V} . \quad (32)$$

Above this voltage, the radiation-induced Joule heating in the ceramic insulator will dominate; below this voltage the dominant effect is nuclear heating. These domains are indicated in Fig. 7.

6. CONCLUSIONS AND RECOMMENDATIONS

6.1 General Conclusions

It has been shown that under absorbed dose-rates typical of fusion reactor conditions, ceramic insulators will exhibit a significant decrease in resistivity. Although these dose-rate-degraded resistivities were seen to be still a factor of $\sim 10^{10} - 10^{12}$ greater than the resistivity of copper, the implications were shown to be important with regard to leakage currents and resulting Joule heating in the ceramic material.

In the case of extruded magnet windings it was shown, by equations 26 and 27 and the results in section 5.1, that the drain on the power supply due to leakage currents is unlikely to be a problem except for very high absorbed doses or very long conductor lengths. However, in section 5.2 it was indicated that the maximum value of these leakage currents may be sufficient to lead to localized thermal runaway in some configurations. For a given absorbed dose-rate, this will depend critically on the design of the magnet or insulator assembly and on the magnitude of the stand-off voltage.

6.2 Edge-Cooled Ribbon Wound Magnets

In the case of unshielded normal-conducting magnets which employ a bare copper alloy ribbon conductor with ceramic insulators between turn-to-turn and layer-to-layer, the effect is expected to be less significant than for a magnet employing an extruded winding due to the relatively low layer-to-layer voltage. In this case, nuclear heating would be expected to be the dominant heating mechanism for any given absorbed dose-rate.

For example, one possible design considered for the normal-conducting insert coil for the MARS⁽²⁾ hybrid mirror solenoid has been a magnet of this type with a terminal voltage V_0 of ~ 6000 V and comprising ~ 25 layers⁽⁴⁾ (i.e., a maximum layer-to-layer voltage of ~ 240 V). Assuming approximately

the same insulator thickness (δ) as that in Fig. 4, it can be seen from Fig. 7 that such a magnet would be operating in the "nuclear heating dominant" regime.

6.3 Magnets Employing Extruded Ceramic Insulation

In the case of magnets wound with extruded conductors of the type considered in sections 4 and 5, the situation is more serious. Here, the ceramic insulation at the high voltage end of the winding is required to stand off the full supply voltage between the center conductor and the outer grounded sheath (see Fig. 3). Due to the relatively low thermal conductivity of the insulator, the maximum heating rate per unit volume will be limited to a few tens of W/cm^3 (and probably to the low end of this range⁽²⁵⁾) although the actual design limit will depend on the heat transfer properties of the winding cross section.

Consider the typical extruded conductor winding shown in Fig. 4. Reference to the set of parametric curves for this winding in Fig. 7 indicates that at an absorbed dose-rate of $\sim 10^4$ Gy/s (certainly not an upper limit for some fusion systems - see section 4), terminal voltages must be reduced below ~ 700 V in order to limit the insulator heating to below $100 \text{ W}/\text{cm}^3$!

6.4 Direct Converter Insulators

In the case of direct converters, which will be incorporated in the end cells of tandem mirror devices (see section 1), there may be a similar problem. Generally, the radiation fields (and thus absorbed dose-rates) in the end cells are considerably less than those in the central cell and barrier/mirror regions. However, the direct converter insulators are required to stand off voltages in the region of tens to hundreds of kV. Therefore, in view of the fact that radiation-induced Joule heating rates scale as V_0^2 (see

equations 14, 15 and 20), leakage currents need to be carefully assessed in any conceptual direct convertor design.

6.5 Methods of Reducing Dose-Rate Conductivity Effects

What methods are available to minimize dose-rate induced conductivity increases and resulting deleterious Joule heating in ceramic insulators? Since, as was shown in section 4, such Joule heating scales approximately as $\sim V_0^2 D_r / \delta^2$, where D_r is the absorbed dose-rate and V_0 is the voltage applied across a characteristic insulator dimension of δ (see equations 14, 15 and 20), it would seem expedient to reduce the first two parameters or increase the latter. Unfortunately, for normal-conducting magnets, there is a design conflict here, since small values of δ are desirable for high conductor packing fractions (i.e., high current densities), while unshielded coils (implying large D_r) are desirable from an economic standpoint (see section 1).

With regard to reducing the supply voltage V_0 , one method is to employ n parallel windings of length ℓ/n , each carrying a current I , rather than one winding of length ℓ carrying this same current. This requires a supply voltage for each separate winding of only $1/n$ of that required in the latter case. However, it also necessitates a current supply bus to the coil capable of a current capacity of n times that of the latter case. Optimum design is, therefore, a trade between several conflicting requirements.

One effective means of reducing dose-rate-induced leakage currents depends on the fact that these currents scale as the product of V_0^2 and D_r . While for an unshielded coil and given first wall neutron environment, the peak value of D_r is fixed, it is important to notice that the coil itself is a good radiation shield. Siting the high voltage portion of the windings at the back of the coil would result in a significantly lower value of D_r for a given value of V_0 .

6.6 The Need for Further Experimental Data

One final important point should be noted in this work. The analysis in this report has been conducted using a relatively simple algorithm for computing dose-rate dependent conductivities (i.e., equation 2). This algorithm is based on experimental data⁽¹¹⁾ for one type of ceramic material (Al_2O_3) in one configuration (single crystal) and for a relatively limited range of absorbed dose-rates induced by one specific radiation type (electrons). How this data translates to other ceramic materials (e.g., MgO , MgAl_2O_4 , Si_3N_4 , etc.) in different configurations (e.g., single crystal, polycrystalline solids, compacted powders, etc.) under different radiation conditions (e.g., energy-dependent neutron and/or gamma fluxes, etc.), is not at all clear. Therefore, in view of the current requirements of the U.S. fusion program, there would appear to be an urgent need for a systematic experimental program, such that adequate parametric data can be obtained on instantaneous dose-rate conductivity effects for a wide range of materials and conditions.

ACKNOWLEDGEMENT

Support for this work has been provided by the U.S. Department of Energy.

REFERENCES

1. Badger, B., et al., "TASKA, A Tandem Mirror Fusion Engineering Facility", UWFDM-500/FPA-82-1/KFK-3311, University of Wisconsin Fusion Engineering Program (1982).
2. MARS - Mirror Advanced Reactor Study. This is a DOE-funded conceptual design study of a ~ 1200 MWe tandem mirror fusion reactor, currently being performed jointly by Lawrence Livermore National Laboratory, University of Wisconsin, TRW, General Dynamics, SAI, Ebasco and Grumman Aerospace Corp. An interim report is to be published in 1982 followed by a final report in 1983.
3. TDF - Tandem Mirror Demonstration Facility. This is a DOE-funded design study of a fusion engineering device based on the tandem mirror principle, and is currently being performed jointly by Lawrence Livermore National Laboratory, University of Wisconsin, TRW, General Dynamics, General Atomic, SAI, Los Alamos National Laboratory and others. A final report will be published in 1982. See also, Fowler, T.K. and Logan, B.G., "Tandem Mirror Technology Demonstration Facility", UCID-19193, Lawrence Livermore National Laboratory (1981).
4. Baldi, B., General Dynamics (Convair Division), San Diego, CA, private communication (1982).
5. Gold, R.E., Bloom, E.E., Clinard, F.W., Smith, D.L., Stevenson, R.D., and W.G. Wolfer, Nuclear Technology/Fusion 1 169 (1981).
6. Perkins, L.J., to be published as a University of Wisconsin Fusion Engineering Program Report (1982).
7. Bussard, R.W. and R.A. Shanny, "Conceptual Design of a Modular Throwaway Tokamak Commercial Fusion Power Plant", Internal Report, INESCO, Inc. (1978).
8. Davis, M.V., in "Nuclear Applications of Non-Fissionable Ceramics", Boltax, A. and J.H. Handwerk, (eds.), (Am. Nucl. Soc., Hinsdale, Illinois, 1966), p. 229.
9. Lynch, G.F., Can. J. Phys. 53, 210 (1975).
10. Clinard, F.W., Los Alamos National Laboratory, private communication, 1982.
11. Klaffky, R.W., et al., Phys. Rev. 8, 21, 3610 (1980).
12. Kaye, G.W.C. and T.H. Laby, "Tables of Physical and Chemical Constants", p. 94 (Longmans, London, 1966).
13. Schultz, J.H., in "Proc. Mtg. on Electrical Insulators Fusion Magnets", p. 4.1, CONF-801237 (DOE, Nov. 1981).
14. Harvey, A., IEEE Trans. Magnetics, MAG-17, No. 5, 1718 (1981).

15. Klaffky, R.W., in "Special Purpose Materials Annual Progress Report for 1979," DOE/ER-0048/1, p. 19, U.S.DOE (1980).
16. Hurley, G.F. and F.W. Clinard, in "Special Purpose Materials Annual Progress Report for 1978," DOE/ET-0095, p. 59, U.S.DOE (1979).
17. Stevanovic, M. and J. Elston, Proc. Br. Ceramics, Soc. 7, 423 (1967).
18. Clinard, F.W., and G.F. Hurley, LA-UR 81-2504, Los Alamos National Laboratory (1981).
19. Van Lint, V.A.J., Bunch, J.M., and T.M. Flanagan in "Radiation Effects and Tritium Technology for Fusion Reactors," p. II-531, CONF-750989, USERDA (1976).
20. Maynard, C.W. and L. El-Guebaly, Fusion Engineering Program, University of Wisconsin, private communication (1982).
21. "An Engineering Design Study of a Reference Theta-Pinch Reactor, RTPR", LA-5336/ANL-8019, Los Alamos Scientific Laboratory/Argonne National Laboratory (1974).
22. Badger, B., et al., "WITAMIR-I, A University of Wisconsin Tandem Mirror Reactor Design", UWFDM-400, Chapter VII, University of Wisconsin Fusion Engineering Program (1980).
23. See Ref. 1, Section VIII.4.
24. Clinard, F.W., J. Nucl. Mater. 85, 86, 393 (1979).
25. Sze, D.K., Fusion Engineering Program, University of Wisconsin, private communication (1982).